Electromagnetic Chirps from Neutron Star-Black Hole Mergers

Jeremy D. Schnittman

NASA Goddard Space Flight Center, Greenbelt, MD 20771

Joint Space-Science Institute, College Park, MD 20742

jeremy.schnittman@nasa.gov

Tito Dal Canton

NASA Postdoctoral Program Fellow, Goddard Space Flight Center, Greenbelt, MD 20771

Jordan Camp

NASA Goddard Space Flight Center, Greenbelt, MD 20771

David Tsang

Department of Astronomy, University of Maryland, College Park, MD 20742

Joint Space-Science Institute, College Park, MD 20742

and

Bernard J. Kelly

CRESST, NASA Goddard Space Flight Center, Greenbelt, MD 20771

Department of Physics, University of Maryland Baltimore County, Baltimore, MD 21250

Joint Space-Science Institute, College Park, MD 20742

ABSTRACT

We calculate the electromagnetic signal of a gamma-ray flare coming from the surface of a neutron star shortly before merger with a black hole companion. Using a new version of the Monte Carlo radiation transport code `Pandurata` that incorporates dynamic spacetimes, we integrate photon geodesics from the neutron star surface until they reach a distant observer or are captured by the black hole. The gamma-ray light curve is modulated by a number of relativistic effects, including Doppler beaming and gravitational lensing. Because the photons originate from the inspiraling neutron star, the light curve closely resembles the

corresponding gravitational waveform: a chirp signal characterized by a steadily increasing frequency and amplitude. We propose to search for these electromagnetic chirps using matched filtering algorithms similar to those used in LIGO data analysis.

Subject headings: black hole physics – accretion disks – X-rays:binaries

1. INTRODUCTION

The tremendous excitement generated by the recent LIGO discoveries of gravitational waves (GWs) from merging binary black holes (Abbott et al. 2016b,a) will only be surpassed by the unambiguous simultaneous detection of an electromagnetic (EM) counterpart to such a GW signal. With an EM counterpart, the sky localization of the GW source will likely be greatly improved, and if a host galaxy can be identified, the event can be placed in the proper astrophysical context. The galaxy's redshift could also be used in conjunction with the luminosity distance—measured independently with the GW signal—to place new and unbiased constraints on cosmological parameters (Nissanke et al. 2010).

Another major advantage of detecting an EM counterpart is that it could give us the ability to combine with sub-threshold GW triggers and improve the statistical significance of marginal signals, potentially lowering the false alarm rate. It is also conceivable that several weak coincident EM and GW signals could reveal a population of sources which are individually too weak to be detectable by blind GW or EM searches.

One of the most promising mechanisms for a LIGO counterpart is a short gamma-ray burst (SGRB) produced by seeing a binary neutron star (NS/NS) or neutron star-black hole (NS/BH) binary merger (Eichler et al. 1989). The disrupted NS will form a massive, highly magnetized accretion disk around the companion BH, driving a relativistic jet which will be manifest as a SGRB to observers oriented along the jet axis. For a sub-sample of SGRBs, a precursor gamma-ray flare can be seen roughly $1 - 10$ seconds before the peak of the GRB (Troja et al. 2010). For a nominal NS/BH binary with masses $1.4M_{\odot}$ and $10M_{\odot}$, this would correspond to hundreds of orbits before merger, with binary separations of $20 - 30$ gravitational radii.

In this paper, we explore the possibility that these precursor flares come from some emission process on the surface of the neutron star as it spirals towards the companion black hole. If so, the resulting gamma-rays will experience the extreme gravitational forces that govern this highly relativistic and dynamical system. These effects will be imprinted on the gamma-ray signal that ultimately reaches a distant observer. We have identified two primary

features in these light curves: special relativistic Doppler beaming, and magnification due to gravitational lensing. As we will show below, the detailed properties of the light curve provide information about the binary separation, inclination angle, and orbital period, giving important information complementary to the GW signal.

The most robust feature of this precursor EM light curve is that is should be locked in phase with the GW signal, also chirping through increasing frequency and amplitude as the system approaches merger. Thus we refer to this particular class of counterparts as "electromagnetic chirps." We fully expect that data analysis tools similar to those used in GW searches may be fruitful in discovering and interpreting such signals in otherwise noisy data from gamma-ray observatories such as the Gamma-ray Burst Monitor (GBM) on Fermi (Dal Canton et al. 2017). We remain intentionally agnostic about the specific physical mechanism that produces the gamma-ray flash on the NS surface, but one promising model is that of resonant shattering flares that occur as the binary orbital frequency sweeps through the eigenfrequencies of the NS normal modes during the moments leading up to merger (Tsang et al. 2012; Tsang 2013). When the quadrupolar crust-core interface mode is resonantly excited by tidal interaction, a huge amount of energy can be deposited into the crust, and ultimately released as gamma-rays.

2. LIGHT CURVES IN BINARY SPACETIME

We calculate the light curves and spectra from the NS/BH system with the Monte Carlo radiation transport code `Pandurata` (Schnittman & Krolik 2013). To date, `Pandurata` has only been applied to problems with stationary Kerr spacetimes. In order to use it for the highly dynamic spacetime of a merging compact binary system, significant modifications were required. First and foremost, we needed to move from the Hamiltonian formalism described in Schnittman & Krolik (2013), appropriate for a system with multiple integrals of motion, to a more generalized Lagrangian approach to solving the geodesic equation for an arbitrary metric and connection, better suited for the binary spacetime.

At the same time, we desired a spacetime formulation that would be computationally efficient for integrating millions of geodesic trajectories. Thus, instead of using full numerical relativity data (typically only available for tens of binary orbits), we instead opted for a relatively simple analytic description of the binary spacetime based on a post-Newtonian (PN) approximation to the orbit (Kelly et al. 2007).

The binary is completely described by two non-spinning point masses with $m_1+m_2 = M$ and $m_1 \geq m_2$, moving on a circular orbit with binary separation $D \equiv (GM/c^2)x$ (unless

explicitly stated otherwise, we hereby assume units with $G = c = 1$). The angular velocity is given by the 2PN expression

$$\Omega = \left[64\frac{x^3}{(1+2x)^6} + \eta\frac{1}{x^4} + \left(-\frac{5}{8\eta} + \eta^2\right)\frac{1}{x^5}\right]^{1/2} M^{-1}\,, \tag{1}$$

with $\eta \equiv m_1 m_2/M^2$.

The orbit is assumed to be instantaneously circular, but we do evolve the separation according to the 2.5PN leading quadrupole radiation reaction terms derived in Peters (1964):

$$\frac{dx}{dt} = -\frac{64}{5}\eta\frac{1}{x^3}\,. \tag{2}$$

The metric is expressed by the standard 3+1 lapse/shift formalism:

$$g_{\mu\nu} = \begin{pmatrix} -\alpha^2 + \beta^2 & \beta_j \\ \beta_i & \gamma_{ij} \end{pmatrix}. \tag{3}$$

Following Campanelli et al. (2006), we use $\alpha = 2/(1+\psi^4)$, $\beta_j = 0$, and $\gamma_{ij} = \delta_{ij}\psi^4$. The conformal factor ψ is given by

$$\psi = 1 + \frac{m_1}{2r_1} + \frac{m_2}{2r_2}\,, \tag{4}$$

with r_1 and r_2 being the simple Cartesian distances between the spatial coordinate and the primary/secondary masses. For the Christoffel components $\Gamma^\rho_{\mu\nu}$ we take the spatial and temporal metric derivatives analytically based on the trajectory as given by equation (1).

To generate light curves, `Pandurata` employs a Monte Carlo ray-tracing scheme that is based on shooting a large number of photon packets from the emission region to potential observers at infinity (Schnittman & Krolik 2013). For the NS/BH problem investigated here, we use a simple thermal, optically thick emission model. Each photon is launched from the surface of the NS with radius 10 km, isotropic in the local frame of the star and with a limb-darkening factor appropriate for an optically thick emitter. This gives the photon's initial position $\mathbf{x}$ and four-velocity $\mathbf{u}$. The photon is then propagated forward along the affine parameter λ according to the standard geodesic formula

$$\frac{d^2x^\rho}{d\lambda^2} = -\Gamma^\rho_{\mu\nu}\frac{dx^\mu}{d\lambda}\frac{dx^\nu}{d\lambda}\,. \tag{5}$$

When a photon packet reaches a simulated detector surface at some large radius, its direction specifies the appropriate pixel in the image plane, exactly like a pinhole camera. Since each photon is also tagged with a time stamp, a movie can be built up over time.

Generally, each observer is located at a specific sky position (θ, ϕ), so the vast majority of the Monte Carlo photons never contribute to the image. For circular orbits, we are able to take advantage of the periodic motion of the binary to efficiently map the azimuthal coordinate to the time coordinate, so a single movie is produced by combining images from observers at all azimuthal positions. Because we are also interested in generating light curves for multiple latitudinal inclination angles, every photon that escapes the system ultimately contributes to some observer's light curve, restoring a remarkable level of efficiency for the Monte Carlo approach.

Fig. 1.— Snapshots of thermal emission from the surface of a $1.4M_\odot$ neutron star orbiting a $10M_\odot$ black hole. The observer is at inclination 90°, edge-on to the orbital plane, and the binary separation is $D = 10M$. In panel (a) the observer, black hole, and neutron star are co-linear, resulting in an Einstein ring around the BH, and producing the peak magnification; in (b) the NS is moving towards the observer with maximum blueshift; (c) shows the strong gravitational lensing of photons that are deflected 180° by the BH; and (d) is the point of maximum redshift.

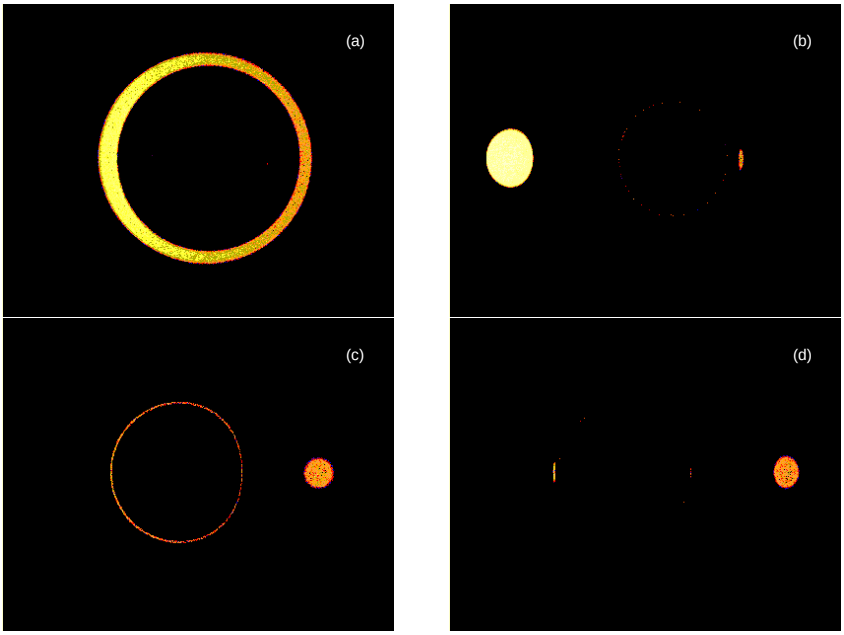

In Figure 1 we show four snapshots of the NS/BH system as seen by an observer oriented edge-on to the orbital plane. The binary masses are $m_1 = 10M_\odot$ and $m_2 = 1.4M_\odot$ and the binary separation is $D = 10M$. The two dominant effects here are gravitational lensing and relativistic beaming. From weak lensing theory, whenever there is co-alignment of the source, lens, and observer, an Einstein ring is formed, with high magnification. Lensing by

a black hole produces an infinite number of concentric Einstein rings, each one at smaller radius and magnification.

The primary Einstein ring can be seen in panel (a), when the NS is on the far side of the BH relative to the observer. The NS then progresses around its orbit to (b), when it reaches the point of maximum blueshift and beaming towards the observer. Also seen in (b) is the faint secondary Einstein ring, only appearing a quarter phase later due to the time delay of photons orbiting around the BH before reaching the observer. In panel (c) another Einstein ring is seen, produced when the system is aligned in the order BH–NS–observer, and the photons from the nearer NS are deflected 180° by the BH on the far side of the orbit before returning to the observer. By this time, the NS has already moved roughly a quarter phase out of the way, and thus does not appear co-linear with the BH. Finally, in panel (d) the NS is at the point of maximum redshift, noticeably fainter than in panel (b).

Fig. 2.— *(top)* Normalized light curve corresponding to Figure 1, with the time of each panel labeled accordingly. *(bottom)* Normalized light curve from the same system, but with binary separation $D = 40M$.

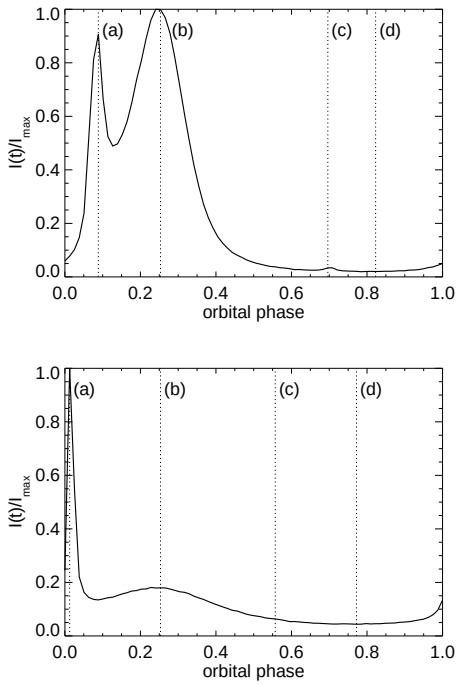

In Figure 2 we show the bolometric light curve corresponding to the snapshots in Figure 1. At this small binary separation of $10M$, the orbital velocity is roughly a quarter of the

speed of light, so the dominant feature in the light curve is the Doppler beaming as the NS moves towards and away from the observer. The lensing magnification contributes a strong peak at (a), and a much smaller peak visible at (c). In the bottom panel of Figure 2 we show the light curve from the same system at binary separation $D = 40M$. The orbital velocity, and thus relativistic beaming effect, is much smaller, while the lensing still produces a large magnification. The smaller orbital velocity also implies the light-crossing time is shorter relative to the orbital period, so the four phases corresponding to those shown in Figure 1 are more evenly spaced in time.

Fig. 3.— Light curve dependence on observer inclination. The binary separation is $10M$ as in Fig. 1. While the relativistic beaming effects are significant even at low inclinations, the lensing effects are only observable above $\sim 80°$.

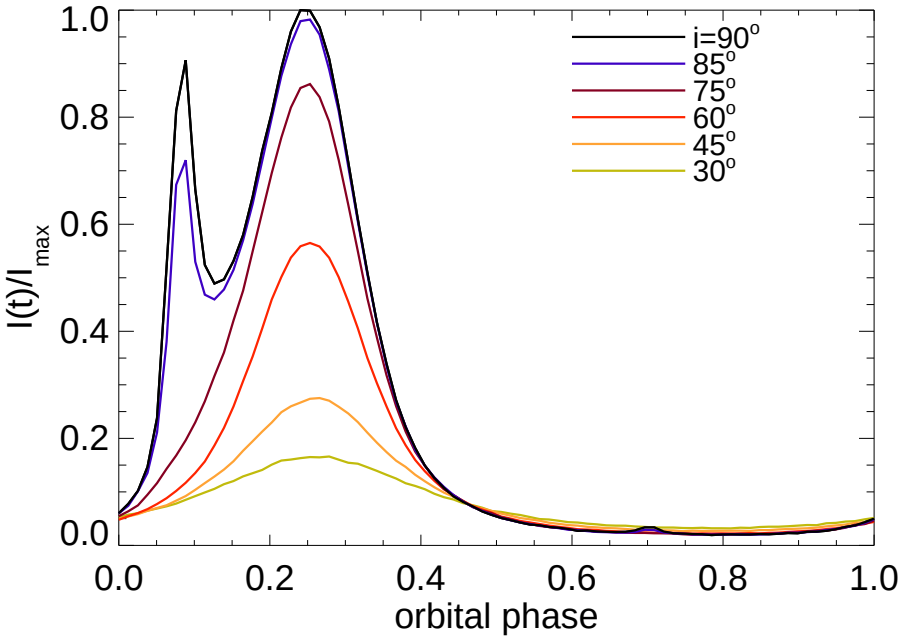

Figure 3 shows the dependence of the light curve features on observer inclination. Not surprisingly, the sharp lensing feature is only visible at high inclination angles with $i \gtrsim 80°$. Yet even at $i = 30°$, the relativistic beaming is responsible for a significant modulation in the light curve. This is because, at a given frequency, the observed flux scales like the redshift cubed: $I_\nu \sim (\nu_{\rm obs}/\nu_{\rm em})^3$. The bolometric flux modulation is greater by another factor of the redshift. One simple way to understand this is when the emitter has a blackbody temperature $T_{\rm em}$, it is observed as a blackbody with temperature $T_{\rm obs} = T_{\rm em}(\nu_{\rm obs}/\nu_{\rm em})$, and

of course the total flux scales like T^4. For even the moderate inclination of $i = 30°$, the ratio of peak-to-valley flux is $I_{\rm max}/I_{\rm min} \approx 3$, while for edge-on systems the modulation is an order of magnitude greater.

Fig. 4.— Light curve dependence on energy. The binary separation is $10M$ as in Fig. 1, and the observer inclination is 60°.

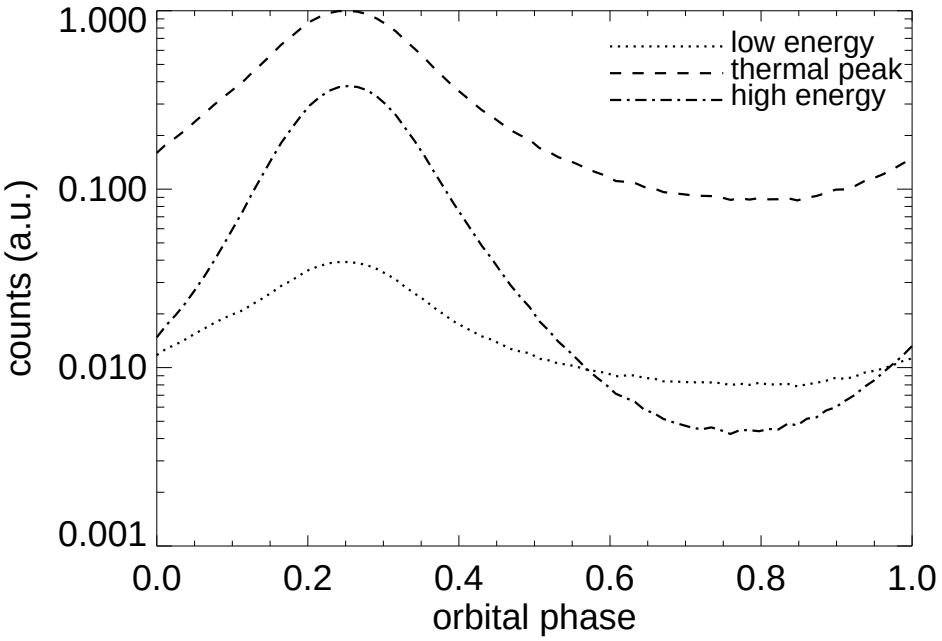

For a thermal emission spectrum, the magnitude of the Doppler modulation also depends on the energy band at which it is observed. At energies below the thermal peak, the slope of the spectrum is increasing like $I_\nu \sim \nu^2$, so the net effect of beaming is relatively modest: the observer sees a blue(red)-shifted portion of an inherently fainter(brighter) part of the spectrum. The opposite is true at energies above the thermal peak, where the relativistic beaming combines with the inherent shape of the spectrum to enhance the effect of Doppler modulation. These effects are shown in Figure 4, where we have divided the observed spectrum into three broad bands, one covering the thermal peak, and one each above and below. For an inclination angle of 60°, the bolometric peak-to-valley amplitude is ~ 10, while the high-energy flux is actually modulated by nearly a factor of 100. This will have important implications for designing a search strategy for these systems.

On the other hand, the gravitational lensing is achromatic, and generally strongest when

the source is moving transverse to the observer, so the lensing modulation will have roughly the same effect on light curves in different energy bands.

3. ELECTROMAGNETIC CHIRPS

As shown in the previous section, the gamma-ray light curve from a NS/BH binary is modulated at the orbital frequency with an amplitude that is a function of the line-of-sight velocity. As the orbit shrinks due to gravitational radiation losses, the frequency and amplitude of the gamma-ray light curve increase. In other words, the EM light curve *chirps*, just like the GW signal.

A NS/BH system with masses $1.4M_\odot$ and $10M_\odot$ will complete roughly 700 orbits during the final minute before merger, entirely within the LIGO band. A portion of the light curve corresponding to this period is shown in Figure 5. To achieve sufficiently high resolution with `Pandurata` over such a long time, we need only calculate a handful of circular light curves, each at a different orbital separation, and then interpolate between them according to the inspiral evolution as governed by equation (2). The evolution is cut off at a separation $D = 10M$, shortly before merger. In practice, the light curve shown in Figure 5 should really be thought of as a *modulation window* to be multiplied by the inherent flare luminosity, which may only last a few seconds or less, depending on the emissivity model.

Fig. 5.— Electromagnetic modulation for an inspiraling NS/BH binary starting at orbital separation $50M$, with observer inclination angle 82°. The insets show zoomed-in views of the beginning and end of the inspiral.

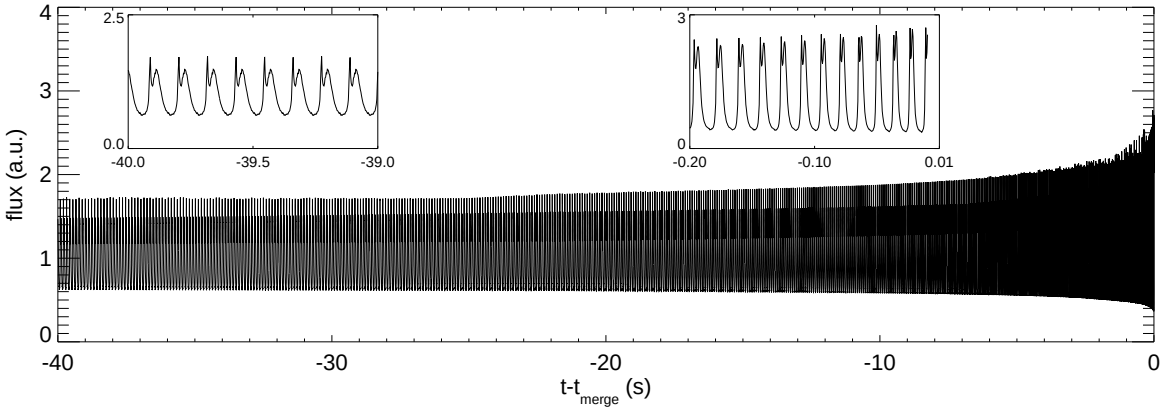

At early times, when the orbital velocity is somewhat smaller, the lensing peak of the

light curve is larger than that due to the Doppler beaming, but at late times the beaming dominates the modulation (see Fig. 2). As with traditional radial velocity observations of spectroscopic binaries, the Doppler shift modulation will provide a degenerate measurement of the BH mass and the binary inclination. For nearly edge-on systems where the lensing peak is observable, the degeneracy can be broken and an accurate BH mass can be determined, much like in the case of transiting exoplanet systems. With a coincident GW detection, the gravitational waveform will provide a different degenerate measure of the binary masses and inclination. For extremely precise light curve measurements, one could even imagine resolving the width of the lensing peak, in turn giving information about the NS radius and thus the equation of state.

There is also the very real possibility that the source could be a NS/NS binary, with either or both neutron stars initiating the gamma-ray flare(s). In this case, the light curve would be simply repeated with half the period, yielding two beaming and two lensing peaks per orbit. Or if the flares occur at different times (potentially due to different NS masses or magnetic field configurations), the light curve would consist of two isolated flares, modulated by the same chirping signature, but offset in phase by 180°.

4. OBSERVATIONAL POTENTIAL

To this point, it has not been necessary to specify the physical mechanism that causes the gamma-ray flare on the NS surface. Anything that leads to emission closely tied to the neutron star will give qualitatively the same EM chirp as the light curves computed in the previous sections. One promising model is that of resonant shattering of the NS crust (Tsang et al. 2012; Tsang 2013). In this scenario, the tidal deformation of the NS, modulated by the orbital motion, resonantly excites the crust-core interface eigenmode, leading to the crust shattering and releasing $\sim 10^{46-48}$ erg on an extremely short time scale. Depending on the NS equation of state, this resonant shattering flare takes place somewhere from 1 to 10 seconds before merger, consistent with SGRB precursors seen with Swift (Troja et al. 2010). Another possible model that similarly deposits a large amount of energy into the NS surface shortly before merger is that of the unipolar inductor, where the accelerating magnetized NS essentially forms an electric generator with the black hole or neutron star companion (Hansen & Lyutikov 2001; Mingarelli et al. 2015; D'Orazio et al. 2016).

We propose to implement efficient searches for these characteristic chirp signals in the data from existing time-domain observatories such as Fermi in conjunction with any LIGO triggers. By using data analysis techniques similar to the matched filtering employed by the LIGO collaboration, we hope to be able to extract long but weak signals from a noisy

background. Moreover, if the source parameters are partially known from a coincident GW signal (in particular the chirp mass and the merger time) then the parameters of the EM chirp are strongly constrained, restricting the volume of parameter space that must be explored and further reducing the false-alarm background of the search, as well as its computational cost. Methods for performing such a search in Fermi/GBM data are currently being investigated and will be described in a companion paper (Dal Canton et al. 2017).

An important caveat in considering the effects of the EM chirp, in the context of these models, is that high luminosities emitted thermally from a small region, like the neutron star surface, will be optically thick to pair-production ($\gamma + \gamma \rightarrow e^+ + e^-$), resulting in a pair-photon fireball that only becomes optically thin at surface of a much larger photosphere (Goodman 1986).

For photons with energies $E_\gamma \approx 500$ keV we can estimate the optical depth to pair production (see e.g., Nakar et al. (2005)):

$$\tau_{\gamma\gamma} \gtrsim \frac{L_\gamma \sigma_T}{4\pi c E_\gamma R_{\rm NS}} \approx 10^{10} \frac{L_\gamma/(10^{46}{\rm erg\,s^{-1}})}{R_{\rm NS}/(10{\rm km})}\,, \tag{6}$$

where L_γ is the luminosity of photons near E_γ and σ_T is the Thompson cross-section. Clearly, if all the energy of these flares is deposited into photons above the pair-production threshold, a relativistic pair-photon fireball is quickly formed, which will expand relativistically until the pair-production freezes out (Goodman 1986), resulting in a large photospheric radius when compared to the orbital and gravitational scales. Additionally, the photospheric surface is accelerated to large Lorentz factor Γ, likely washing out any beaming effects from the orbital dynamics.

For black-body emission, luminosity greater than $L \gtrsim 10^{42}$ erg s^{-1}, when confined to $R_{\rm NS} \approx 10$km ($T \gtrsim 20$keV), will have a sufficiently high-energy tail to be optically thick to pair production. Thus, there exists an unfortunate trade-off for potential EM chirp sources. Those brighter than $L \gtrsim 10^{42}$ erg s^{-1}, which are more easily detectable, will likely be optically thick to pair-production and result in a pair-photon fireball, potentially masking the EM chirp signature. Meanwhile, those with luminosities below this threshold will be more difficult to detect at extra-galactic distances. However, non-thermal emission lacking significant contribution above the pair-production threshold may avoid this limitation.

Resonant shattering flares, with luminosities of $\sim 10^{47-49}$ erg s^{-1}, consistent with the observed SGRB precursors, are likely pair-photon fireballs. However, emission from a black hole or neutron star companion crossing the NS magnetic field lines in the unipolar inductor model are significantly less energetic, with maximum luminosity scaling as $L \sim 10^{40}$ erg s^{-1} $(B/10^{12}{\rm G})^2 (D/10^7{\rm cm})^{-7}$, where B is the NS magnetic field and D the binary separation (Hansen & Lyutikov 2001).

Despite these potential complications, we are confident that the basic EM chirp remains a robust and potentially very powerful prediction for a counterpart to the GW signal from merging NS binaries. In the near future, we encourage any wide-field survey with sufficiently high time resolution to look for these characteristic chirps preceding GW triggers. In the more distant future, we look forward to using low-frequency GW observatories such as LISA to identify precursor signals that would in turn give an early warning for the time and sky location for ground-based events, triggering more sensitive targeted EM observations (Sesana 2016).

Acknowledgments

This work was partially supported by NASA grant ATP13-0077. TDC was supported by an appointment to the NASA Postdoctoral Program at the Goddard Space Flight Center, administered by Universities Space Research Association under contract with NASA.

REFERENCES

Abbott, B. P., Abbott, R., Abbott, T. D., et al. 2016a, Physical Review Letters, 116, 241103

—. 2016b, Physical Review Letters, 116, 061102

Campanelli, M., Lousto, C. O., & Zlochower, Y. 2006, Physical Review D, 74, 041501(R)

D'Orazio, D. J., Levin, J., Murray, N. W., & Price, L. 2016, Phys. Rev. D, 94, 023001

Eichler, D., Livio, M., Piran, T., & Schramm, D. N. 1989, Nature, 340, 126

Goodman, J. 1986, ApJ, 308, L47

Hansen, B. M. S., & Lyutikov, M. 2001, MNRAS, 322, 695

Kelly, B. J., Tichy, W., Campanelli, M., & Whiting, B. F. 2007, Physical Review D, 76, 024008

Mingarelli, C. M. F., Levin, J., & Lazio, T. J. W. 2015, ApJ, 814, L20

Nakar, E., Piran, T., & Sari, R. 2005, ApJ, 635, 516

Nissanke, S., Holz, D. E., Hughes, S. A., Dalal, N., & Sievers, J. L. 2010, ApJ, 725, 496

Peters, P. C. 1964, Physical Review, 136, 1224

Schnittman, J. D., & Krolik, J. H. 2013, ApJ, 777, 11

Sesana, A. 2016, Physical Review Letters, 116, 231102

Troja, E., Rosswog, S., & Gehrels, N. 2010, ApJ, 723, 1711

Tsang, D. 2013, ApJ, 777, 103

Tsang, D., Read, J. S., Hinderer, T., Piro, A. L., & Bondarescu, R. 2012, Physical Review Letters, 108, 011102